Characteristics, trend, and precursors of extreme cold events in northwestern North America

Jian Shi [a,b,*], Kaijun Wu [c], Weihong Qian [d,e], Fei Huang [a,b], Chun Li [a,b], Cong Tang [a,b]

[a] Key Laboratory of Physical Oceanography, Institute for Advanced Ocean Study, Ocean University of China and Qingdao National Laboratory for Marine Science and Technology, Qingdao, China
[b] College of Oceanic and Atmospheric Sciences, Ocean University of China, Qingdao, China
[c] Department of Aviation Meteorology, Civil Aviation University of China, Tianjin, China
[d] Department of Atmospheric and Oceanic Sciences, School of Physics, Peking University, Beijing, China
[e] Guangzhou Institute of Tropical and Marine Meteorology/Guangdong Provincial Key Laboratory of Regional Numerical Weather Prediction, CMA, Guangzhou, China

ABSTRACT

The cold extremes along with record snowfalls in North America (NA) have attracted great concern for decades. In this study, we select 23 wintertime cold extremes in northwestern NA (NWNA) from 1981 to 2018 and find a significant weakening trend of their integrated yearly intensities. Strong northerlies and cold advections over NWNA associated with the cold events are driven by the intensified and southward Beaufort anticyclone at lower troposphere and the enhanced blocking high at higher levels. A strong low-pressure anomaly over NWNA extends from lower troposphere to stratosphere centered at around 250–300hPa, where the jet stream becomes stronger and moves northwestwards. Meanwhile, the cold anomaly under the low system is deep and more prominent at the surface of NWNA. There is a significant meridional dipole structure of height and temperature anomaly in mid-high latitudes, indicative of the negative phase of Arctic Oscillation. Results further suggest that the La Niña-like sea surface temperature anomalies may serve as a precursor for the cold extremes in NWNA, triggering a Pacific North America-like wave train including an active negative height anomaly center over NWNA, which is linked with the cold anomalies extending downward to the surface. However, the sea ice concentration anomalies in Arctic region and the snow cover anomalies in NA continent during early autumn are likely to exert a minimal influence on the wintertime cold extremes in NWNA.

1. Introduction

The cold extremes along with record snowfalls in the mid-latitude Eurasian and American continents have attracted great attention in the recent decades, motivated by their strong societal and economic impacts as well as the loss of life (e.g., Kodra et al., 2011; Guirguis et al., 2011; Coumou and Rahmstorf, 2012; Grotjahn et al., 2016). In this study, we focus on the cold extremes in the northwestern North America (NWNA; Fig. 1) region, which is a crucial genesis location for Arctic air mass and its associated anticyclone (Zishka and Smith, 1980; Turner and Gyakum, 2011) and exhibits large temperature variability (e.g., Lin and Brunet, 2009).

The weather and climate anomalies in boreal winter are largely influenced by atmospheric circulation patterns in middle and high latitudes of Northern Hemisphere (NH) (e.g., Wang et al., 2010; Guirguis

et al., 2011). The Pacific-North America (PNA) pattern is a prominent low-frequency wave train in the NH extratropics which reflects a quadripole located in the vicinity of Hawaii, south of the Aleutian Islands, intermountain region of North America, and the southeastern United States, respectively (Chen and van den Dool, 2003). The Arctic Oscillation (AO) denotes the fluctuation of low pressure in high latitudes and high pressure in middle latitudes (Hurrell, 1995; Thompson and Wallace, 2001). The North Atlantic Oscillation (NAO) is the dominant mode of winter climate variability in the North Atlantic region ranging from central North America to Europe and much into Northern Asia (Barnston and Livezey, 1987). The NAO is also a large-scale seesaw circulation pattern between the subtropical high and the polar low. The similarities and differences between the AO and NAO are still hotly debated (e.g., Itoh, 2008). Some studies proposed that AO and NAO are synonyms with different names but for the same variability (Wallace,
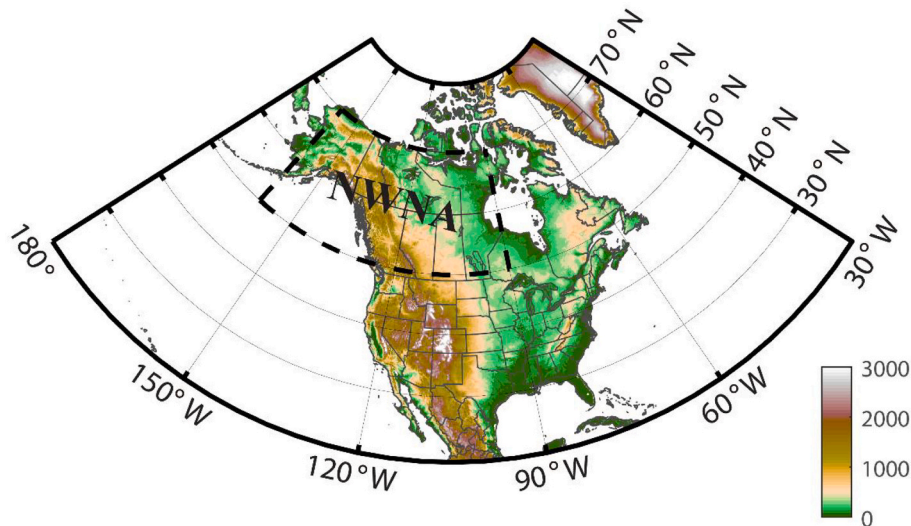
Fig. 1. The topography (shading, in meter) and location of the focused area (dashed box) in the northwestern North America (NWNA).

2000). The AO is an annular mode with the strongest signal located in the Atlantic sector while the NAO is mostly interpreted as a regional pattern controlled by Atlantic processes. These three pivotal circulation patterns are possibly linked to the cold extremes of NWNA. In addition, the variations of traditional meridional cells, the Ferrel cell, Polar cell, and Arctic cell (Qian et al., 2017), may also play a part in the cold surges in NWNA, which need further investigations.

In terms of the precursors favorable for the cold extremes of NWNA, we mainly explore the potential effects of El Niño-Southern Oscillation (ENSO) from tropical Pacific, sea ice from the Arctic Ocean, and snow cover in NA continent. Many studies have noticed the close relationship between ENSO and NA wintertime temperature (Ropelewski and Halpert, 1986; Derome et al., 2001; Mo, 2010; Yu et al., 2012). Papineau (2001) reported that the La Niña winters can produce significant below normal temperatures statewide Alaska. Westby et al. (2013) further stated that the ENSO variations generally operate in conjunction with PNA-like teleconnection to influence the NWNA temperatures.

In higher latitudes, the more frequent and severe cold events are coincident with the accelerating Arctic sea ice loss (e.g., Stroeve et al., 2012) and Arctic amplification (e.g., Cohen et al., 2014; Horton et al., 2015) under the framework of "Warm Arctic, Cold Continents" pattern (Overland et al., 2011; Cohen et al., 2013, 2014; Sun et al., 2016; Luo et al., 2019, 2020). Some studies conjecture that the Arctic sea ice and related atmospheric variabilities in storm track, jet stream, and planetary waves drive the cooling over midlatitude continents (Francis and Vavrus, 2012; Honda et al., 2009; Liu et al., 2012; Cohen et al., 2014; Mori et al., 2014; Kug et al., 2015). However, others hold that there are no significant linkages (Kumar et al., 2010; Gerber et al., 2014; Perlwitz et al., 2015; Li et al., 2015; Sun et al., 2016) or even fewer cold air outbreaks with the decline of Arctic sea ice (Screen et al., 2015; Gao et al., 2015). Moreover, the snow cover, a requirement for the formation of cold air masses (Walsh et al., 2001; Portis et al., 2006; Emanuel, 2008), is also an important factor for cold surges (Vavrus, 2007; Gao et al., 2015) despite its large uncertainty (Peings et al., 2013; Cohen et al., 2014). Specifically, the snow cover may affect the North American cold events by inducing the stratospheric polar vortex anomalies and a persistent negative phase of the tropospheric AO (Cohen et al., 2007; Cohen and Jones, 2011). Considering the special geographic location of NWNA, the Arctic sea ice and terrestrial snow cover could be potentially related to the occurrences of cold events there, which needs further evidence.

In this study, we mainly address three questions for the cold extremes in NWNA: 1) Their statistical characteristics from a historical view: time, duration, intensity, spatial distribution of surface air temperature (SAT)

anomaly, and trend; 2) Their associated winds, vertical height-temperature configuration, and connections with the major circulation and teleconnection patterns; and 3) Their potential driving factors: ENSO, Arctic sea ice, and snow cover over the NA continent. The rest of the paper is organized as follows. The datasets and methods are described in section 2. We illustrate the features and trend of NWNA cold extremes in section 3. Then, we discuss the wind and three-dimensional circulation anomalies in section 4. We further provide some potential precursors for the cold extremes in section 5. A summary and discussion are presented in section 6.

2. Data and methods

We use daily-mean data in this study to describe the cold extremes in NWNA. The atmospheric reanalysis dataset is the National Centers for Environmental Prediction/Department of Energy (NCEP/DOE) Reanalysis 2 (NCEP R2) product from 1979 to the present. The data are obtained from the website (http://www.esrl.noaa.gov/psd/data/gridded/data.ncep.reanalysis2.html) with a horizontal resolution of 2.5° longitude-latitude grids and 17 vertical levels (Kanamitsu et al., 2002). Geopotential height H, temperature T, sea level pressure (SLP), surface winds (u, v) at 10m, and SAT at 2m are used in this study. The monthly gridded SST data are HadISST1 (Rayner et al., 2003) while sea ice concentration (SIC) data are in version 2.2.0.0 (Titchner and Rayner, 2014), both with a $1° \times 1°$ horizontal resolution. This product is a unique combination of global SST and SIC. The data can be retrieved from the website (http://www.metoffice.gov.uk/hadobs/hadisst/ and https://www.metoffice.gov.uk/hadobs/hadisst2/), respectively. The monthly snow cover data are derived from the fifth generation reanalysis of European Centre for Medium-Range Weather Forecasts (ECMWF) (ERA5; Hersbach et al., 2020), which can be downloaded at website (https://cds.climate.copernicus.eu/cdsapp#!/dataset/reanalysis-era5-single-levels-monthly-means?tab=form). The horizontal resolution of snow cover is 0.25° in longitude-latitude grids. We calculate the daily or monthly climatology averaging from 1981 to 2010 (e.g., Qian et al., 2016; Shi and Qian, 2016). The anomalies are defined as the deviations from the corresponding climatology. We choose the period from 1981 to 2018 in this study. The extended winter includes November and December as well as following January, February, March, and April. The long-term trends of variables are retained in this study.

The daily PNA, AO, and NAO indices are obtained from Climate Prediction Center (CPC) of NCEP, which can be accessed at the website (https://www.cpc.ncep.noaa.gov/products/precip/CWlink/daily_ao_index/teleconnections.shtml). In terms of the intensity indices of Ferrel

Table 1

Persistent (at least 5 days) regional (exceeding 1.8×10^6 km^2) cold anomaly (lower than -12°C) events with lifetime, durations (unit: days), total intensity, and rank in the NWNA during extended winter (Nov-Dec-Jan-Feb-Mar-Apr) from 1981 to 2018. The integrated intensity (unit: 10^6 km^2·°C) is calculated as the sum of daily coverage (10^6 km^2) multiplied by daily mean intensity (°C) during the lifetime. The rank is based on the integrated intensity.

Year	Start date	End date	Duration	Integrated intensity	Rank
1981/82	Dec 28	Jan 09	13	-544.7	2
1981/82	Jan 15	Jan 23	9	-477.7	3
1983/84	Dec 15	Dec 24	10	-358.2	9
1984/85	Dec 22	Dec 30	9	-396.2	8
1984/85	Feb 07	Feb 13	7	-220.0	15
1985/86	Nov 22	Dec 01	10	-475.1	4
1988/89	Jan 28	Feb 03	7	-399.1	6
1989/90	Jan 27	Feb 17	22	-846.2	1
1993/94	Jan 04	Jan 09	6	-183.9	20
1993/94	Jan 13	Jan 17	5	-183.1	21
1993/94	Feb 19	Feb 26	8	-312.1	10
1994/95	Mar 03	Mar 07	5	-189.2	19
1995/96	Dec 05	Dec 12	8	-290.5	12
1995/96	Jan 13	Jan 21	9	-431.1	5
1995/96	Jan 27	Feb 02	7	-298.2	11
1996/97	Dec 22	Dec 30	9	-398.0	7
1996/97	Jan 23	Jan 27	5	-181.8	22
2000/01	Dec 10	Dec 16	7	-261.4	13
2001/02	Jan 20	Jan 27	8	-257.7	14
2003/04	Jan 26	Jan 30	5	-197.3	18
2004/05	Jan 12	Jan 16	5	-175.0	23
2007/08	Feb 06	Feb 10	5	-210.0	17
2011/12	Jan 16	Jan 20	5	-215.2	16

cell, Polar cell, and Arctic cell, we use the meridional mass stream function (MSF), which has been used in many previous studies (Lindzen and Hou, 1988; Mitas and Clement, 2005; Hu and Fu, 2007; Qian et al., 2015a, 2017).

In this paper, we analyze the cold extremes located in NWNA (50–70°N, 90–160°W; Fig. 1). A cold extreme is characterized by its intensity, coverage, and duration. According to previous studies (e.g., Vavrus et al., 2006; Wheeler et al., 2011; Smith and Sheridan, 2018, 2020), we tailor the criteria and define a cold extreme in NWNA when it satisfies: 1) covering an area larger than 1.8×10^6 km^2 with daily SAT anomaly reaching -12°C with respect to the corresponding daily climatology, and 2) persisting for more than five consecutive days with at most one-day interruption. The integrated intensity is calculated as the summation of daily coverage (10^6 km^2) multiplied by daily mean intensity (°C, mean SAT anomaly averaged over above area) during the lifetime of a cold extreme. There are 23 cold events based on our criteria from 1981 to 2018 with the detailed information listed in Table 1. They are further ranked according to the integrated intensity. Note that the above events are mostly consistent with the events derived from ERA5 dataset (not shown).

3. Characteristics and trend of cold extremes in NWNA

Figure 2 illustrates the time series of top three cold extremes in the record. The strongest event occurred in 1990 from 27 January to 17 February (pink shading), lasting for 22 days. On 30 January 1990, the average cold anomaly over NWNA could reach around -19°C. The second and third strongest events were in the 1981/82 boreal winter with only one-week break. But these two events were due to different cold air outbreaks from higher latitudes. Note that these three events were relatively steady with slow moving speed (black line in Fig. 2), which would have persistent impacts on local area.

For the timing of cold extremes (Table 1), 7 events occurred in the 1980s and 10 events were in the 1990s, which accounts for more than 2/3 of total events. After 2000, five events occurred in the 2000s while only one event occurred after 2010. Based on this, we could deduce a declining trend of the number of cold extremes. Furthermore, we

calculate the interannual variation of integrated intensity over the whole lifetime of each event (Fig. 3). The integrated intensity also demonstrates a statistically significant weakening trend for the cold extremes. Strong cold extremes are more frequent before mid-1990s, which is consistent with Fig. 2 and Table 1. The large wintertime values in 1981, 1993, and 1995 are contributed by several separate cold events (Fig. 3 and Table 1). The trend calculation here gives a complete picture of temperature extremes with intensity, coverage, and duration considered rather than only a single threshold involved (e.g., Gleason et al., 2008). This weakening trend does not have conflicts with the frigid temperatures over NA and Europe in recent winters, such as 2009/2010, 2010/2011, and 2013/14, which has been widely reported by social media and researchers (e.g., Cattiaux et al., 2010; Wang et al., 2010). Because while some parts of NA and Europe experienced cold surges, the NH was not anomalously cold (Guirguis et al., 2011). The fact was that extreme wintertime warm events were more dominated in both magnitude and spatial coverage. Moreover, above weakening trend of cold events in NWNA is not incompatible with the "Warm Arctic, Cold Continents" trend pattern because our focused NWNA region is located along the boundary region of warming and cooling latitudinal bands (Sun et al., 2016). Rather, this weakening trend well corresponds to the local (Jones and Moberg, 2003; Serreze and Francis, 2006) and global warming (Cassano et al., 2011, 2016). Similarly, the long-term trends toward milder and less frequent cold waves across the US (Peterson et al., 2013) and midlatitude regions (van Oldenborgh et al., 2019) have been revealed.

In terms of the months of the events, around 50% emerged in January and six events started in December, implying a higher possibility of cold extremes to fall within the climatological wintertime. No extreme event occurred in April. In addition, the longest event persisted for 22 days, which would have dramatic impacts on life and agriculture. Other events were less than 2 weeks, consistent with the timescale of biweekly internal variability of atmosphere.

The horizontal distributions of SAT anomalies are shown for the three strongest cold events on the day with the maximum coverage (Fig. 4). On 30 January 1990, the most dominant cold anomalies were mostly located within our targeted area with the magnitude exceeding -25°C (Fig. 4a). The eastern NA to the north of Great Lakes region was experiencing an anomalous warm period (Fig. 4a). There was no outstanding anomalous signal over the wide southern NA (Fig. 4a). On 8 January 1982, cold anomalies prevailed over most of the NA continent with the strongest center of cold anomaly in the NWNA region (Fig. 4b). In Fig. 4c, a dipole of northwest cold and southeast warm was clear on 20 January 1982. It should be noted that these three cold events were not well documented in previous studies. The specific distributions of warm and cold anomalies are different for each event, which may partly result from the intensity of cold air mass and its moving track, but their cold centers are concentrated in the NWNM region for all the 23 cases. In addition, the magnitude of the NWNA cold anomalies is a bit stronger than that in Turner et al. (2013).

4. Wind and circulation features associated with the cold extremes in NWNA

To explore the meteorological features associated with the cold extremes, we firstly show the SLP and winds at surface by performing the composite analysis (Fig. 5). In Fig. 5a, the Beaufort anticyclone stretches southward and merges with the continental anticyclone over NA. This intensified and meridional-elongated anticyclone drives strong northerlies over the NWNA region (also see Fig. 5b). The anomalous northerlies indicate cold advections responsible for these regional cold temperatures (Fig. 5b). Note that other studies have reported the weakening of the Beaufort High, which is consistent with weakening trend of the cold events in NWNA (Fig. 3; Wu et al., 2014; Castruccio et al., 2019; Urrego-Blanco et al., 2019; Zhang et al., 2019). In North Pacific, the Aleutian low is also prominent but shift westwards (Fig. 5).
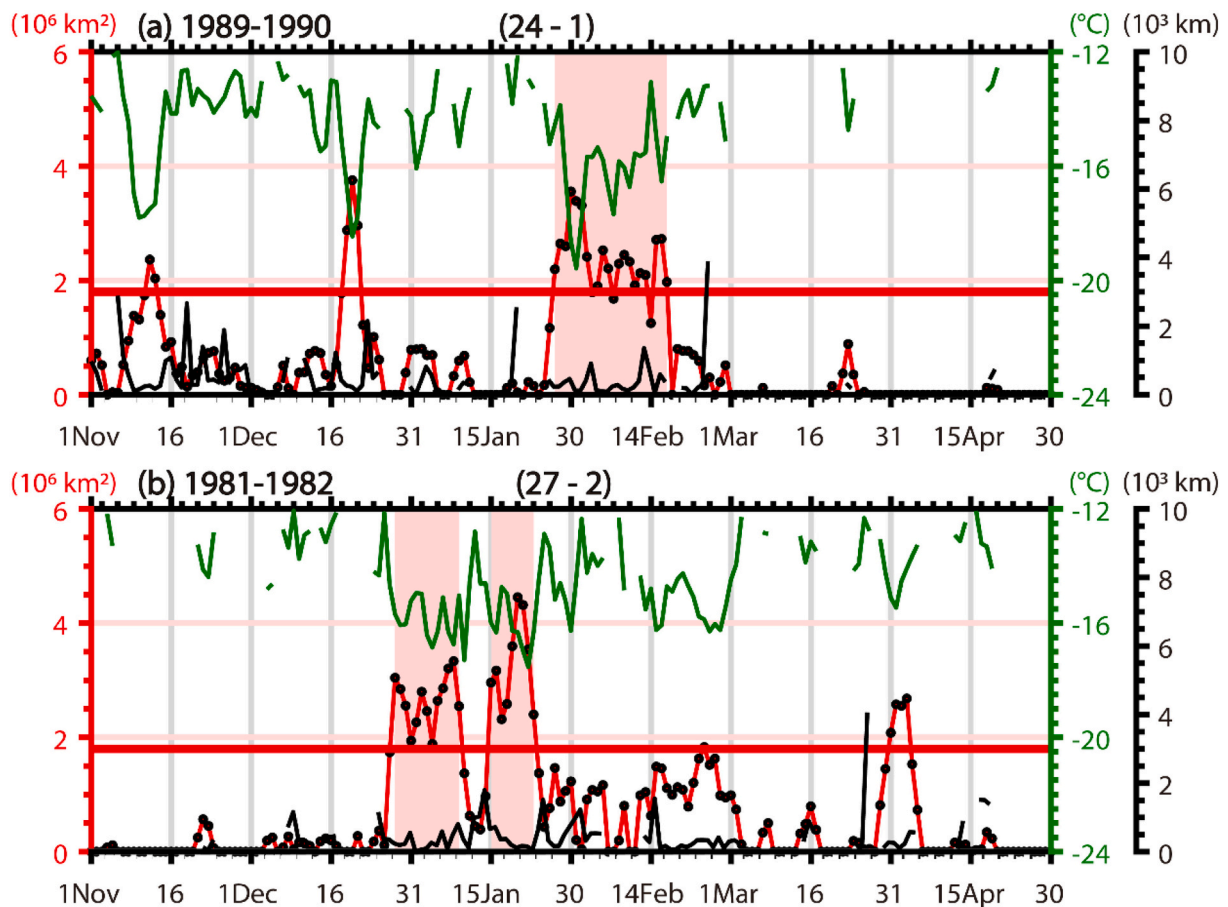
Fig. 2. Daily variations of the average intensity (green line, in °C) with SAT anomalies exceeding -12°C within the NWNA, the coverage (red line with dots, in 10^6 km^2), and the distance (black line, in 10^3 km) between anomalous temperature centers in two adjacent days. The daily anomalous center is defined by the centroid weighted by the magnitude of SAT anomalies within the NWNA area. The lifetime of three strongest cold events is highlighted by pink shading in (a) 1989/90 winter and (b) 1981/82 winter. The thick red lines denote the 1.8×10^6 km^2 coverage (e.g., the coverage threshold). The numbers within the bracket in the middle top indicate the number of days with coverage larger than 1.8×10^6 km^2 and the number of cold events, respectively.

This intense baroclinic high-low pressure couplet and associated cold-air damming (Fig. 4) are consistent with Turner and Gyakum (2011).

We further probe into the horizontal height pattern in upper levels (Fig. 6). At 300hPa, a robust mid-latitude wave train is detected which includes a strong low anomaly over NWNA and an anomalous high ridge over northeast Pacific extending into the Arctic region (Fig. 6a). The favorable conditions for severe winters in NWNA are similar to those in Kug et al. (2015). In terms of the jet stream, it becomes stronger and wider and moves northwestwards (Fig. 6a). The stronger temperature and height gradients reinforce the jet stream and baroclinity while the northwestward movement of the Alaska ridge drives the westward shift of jet stream (not shown). On the left side of jet entrance around the NWNA, there is a negative vorticity advection and a cyclonic shear vorticity, which are in favor of the development and persistence of surface anticyclone as shown in Fig. 5. At 500hPa, the enhanced ridge over Aleutian Islands and Alaska extends into the central Arctic region,

driving strong cold advection into NWNA (Fig. 6b). The above developing blocking high establishes a meridional circulation pattern over North Pacific and NWNA area (Fig. 6b), indicative of the longer duration and strong intensity of cold events. This stable blocking condition is vital for mid-latitudes cold extremes (Sillmann et al., 2011; Yao et al., 2017; Li et al., 2020; Luo et al., 2018, 2020) and also has implication for the weather prediction for eastern North America.

In terms of the responsible teleconnections, there is a prominent PNA-like teleconnection originating from tropical Pacific and propagating towards Aleutian Islands, NWNA, and southern NA (Fig. 6b). Moreover, the general opposite height anomalies in polar and midlatitude regions suggest a negative phase of AO. The out-of-phase height pattern with low anomaly in NWNA and high anomaly poleward favors the penetration of cold air into NWNA. The height oscillation between high and middle latitudes are only significant in eastern Eurasia and NA sector (Fig. 6). In North Atlantic, the height anomalies
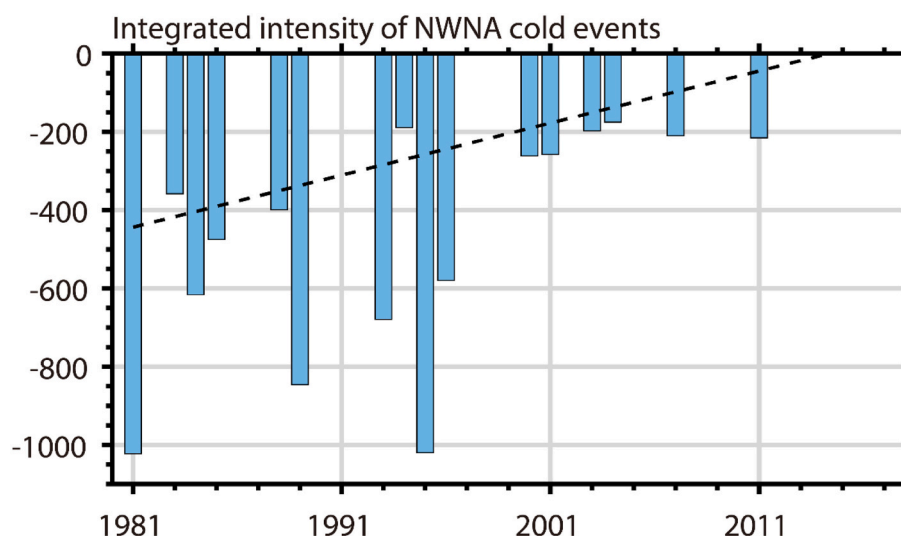
Fig. 3. The interannual variation of integrated intensity of cold events in NWNA from 1981 to 2018. The integrated intensity for each year is the sum of the product of intensity and coverage over the whole lifetime of each event. The dashed line indicates a weakening trend of the integrated intensity. The trend exceeds 95% confidence level of student's *t*-test. The year 1981, for example, indicates the 1981/1982 extended winter (November to April).

are much weaker and only significant in middle latitudes. Above results are further proved in Table 2, which calculates the composite values of synchronous daily PNA, AO, and NAO for the selected cold extremes in the NWNA region. The PNA and AO are significantly negative and provide favorable atmospheric conditions for the cold extremes. However, the NAO plays a negligible role, probably resulting from its remote distance to the NWNA region (Table 2). The salient role of AO in NWNA region is somewhat different from the US and Europe, where NAO is more important during the cold outbreaks (Walsh et al., 2001).

We also compute the composite intensities of the three meridional cells averaged over the lifetime of NWNA cold extremes (Table 2). The cold events are only connected with the reinforced Polar cell significantly, possibly contributed by the dipolar height anomalies for positive polar and negative mid-latitude bands. Nevertheless, as the three circulation indices are zonally averaged, which may not well explain the regional cold events, we further calculate the intensity of Polar cell averaged within the NWNA sector. But the sectorial-averaged Polar cell is not statistically significant, indicating that the regional Polar cell may not greatly influence the cold events in NWNA. The potential connection between the meridional cells and regional cold events is seldom documented by previous studies.

Then, we illustrate the vertical cross sections of height and temperature anomalies along the central longitude 120°W for the three strongest cold events (Fig. 7). For the strongest event, an anomalous low was predominant over the mid-latitude troposphere up to 100hPa on 30 January 1990 (Fig. 7a). The center of the anomalous low was at upper troposphere around 300hPa accompanied by a strong cold air column extending and intensifying downward to the surface associated with the surface cold temperature. On 8 January 1982, although the high and low anomalies alternated meridionally, an anomalous low was located above the focused NWNA region with its center at 300hPa (Fig. 7b). The cold column below the low center was strongest at surface. Two weeks later on 20 January 1982, another low system dominated the lower and middle latitudes within the whole troposphere (Fig. 7c). The cold anomalies were prevalent within the whole NH troposphere with the strongest anomaly at the surface of NWNA region, in accordance with a deep-layer cooling as documented in Turner and Gyakum (2011).

Further, the composite height-temperature cross section averaged over the whole lifetime for all the events are calculated (Fig. 8). The anomalous low system is statistically significant and covers a large area from lower troposphere to stratosphere centered at around 250–300hPa. The cold anomaly under the low anomaly is prominent at surface which

corresponds to the cold extremes in NWNA. From surface up to 850hPa, a weak high anomaly exists as shown in Fig. 5, consistent with the three individual events in Fig. 7. Moreover, the low system, the cold anomaly below, and the warm anomaly above satisfy the hydrostatic balance as shown in previous studies (Qian et al., 2015b, 2016). In addition, there is a significant height dipole in mid-high latitudes, which is also manifested in Fig. 7. These results imply that anomalous atmospheric circulation may drive cold winters in NWNA and mild Arctic conditions, in agreement with that in Blackport et al. (2019).

For the perspective of the evolution of these events, the high system in North Pacific established one week before the peak day (Fig. 9a) and developed into the blocking state due to the warm-advection conveyor westward behind (Fig. 9b–d), reaching its maximum on the peak day. After that, the blocking high gradually broke (Fig. 9e, f) and the severity of cold events also decreased. The persistence of the blocking is also related to the slow moving of temperature anomalies in NWNA area (black line in Fig. 2).

5. Potential precursors for the cold extremes in NWNA

In this section, we further reveal the potential roles of SST anomalies (Fig. 10), sea ice concentration (SIC) anomalies (Fig. 11a), and snow cover anomalies (Fig. 11b) in driving cold extremes in NWNA. In preceding summer and autumn, the anomalous SST pattern is featured by a prominent La Niña-like cooling over central-eastern tropical Pacific (Fig. 10a). The SST anomalies in this region further intensify to its peak phase in following seasons and persist for at least 10 months in total (Fig. 10b). As previous studies suggest (Papineau, 2001; Westby et al., 2013), the La Niña-like SST anomalies can trigger a PNA wave train in its negative phase. One of the active centers of the PNA response with negative height anomalies is located above the NWNA region, which is linked with the negative temperature anomalies extending downward to the surface (Figs. 6b, 8). This large-scale SST pattern acts as a stable and favorable background, but not sufficient and not a necessary condition (not shown), for the occurrence of cold extremes in NWNA. In Atlantic, there is almost no significant signal related to the cold extremes in NWNA.

As mentioned in Introduction, the role of SIC on wintertime cold extremes in Eurasian and NA continents is hotly debated (Honda et al., 2009; Kumar et al., 2010; Mori et al., 2014; Gerber et al., 2014; Kug et al., 2015; Perlwitz et al., 2015; Li et al., 2015; Gao et al., 2015; Screen et al., 2015; Blackport et al., 2019), but no consensus has been reached
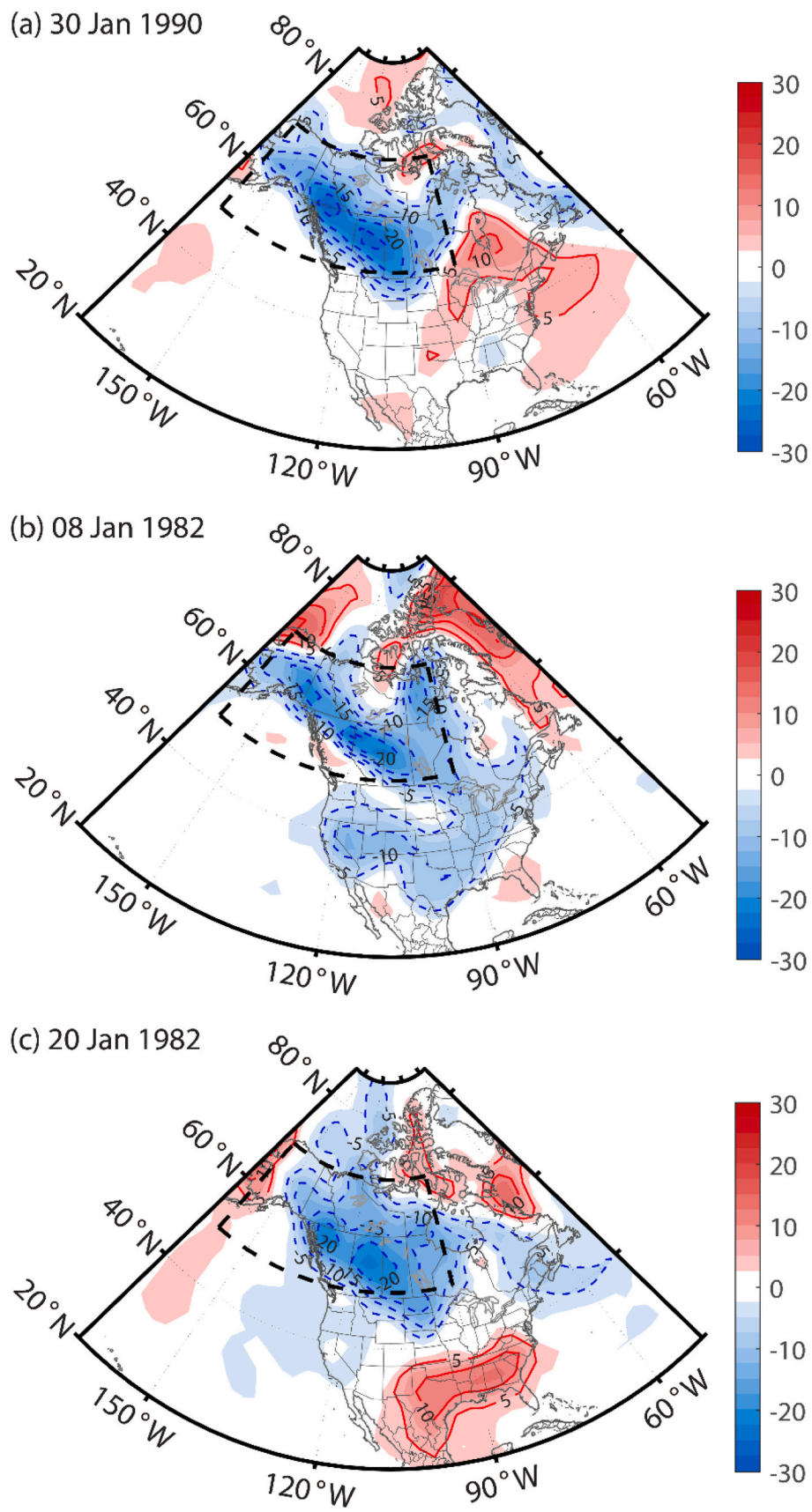
(a) 30 Jan 1990

(b) 08 Jan 1982

(c) 20 Jan 1982

Fig. 4. The SAT anomalies (shading with contour, in °C) on the day with the maximum coverage of the top three strongest cold events. The black dashed lines outline the NWNA region.
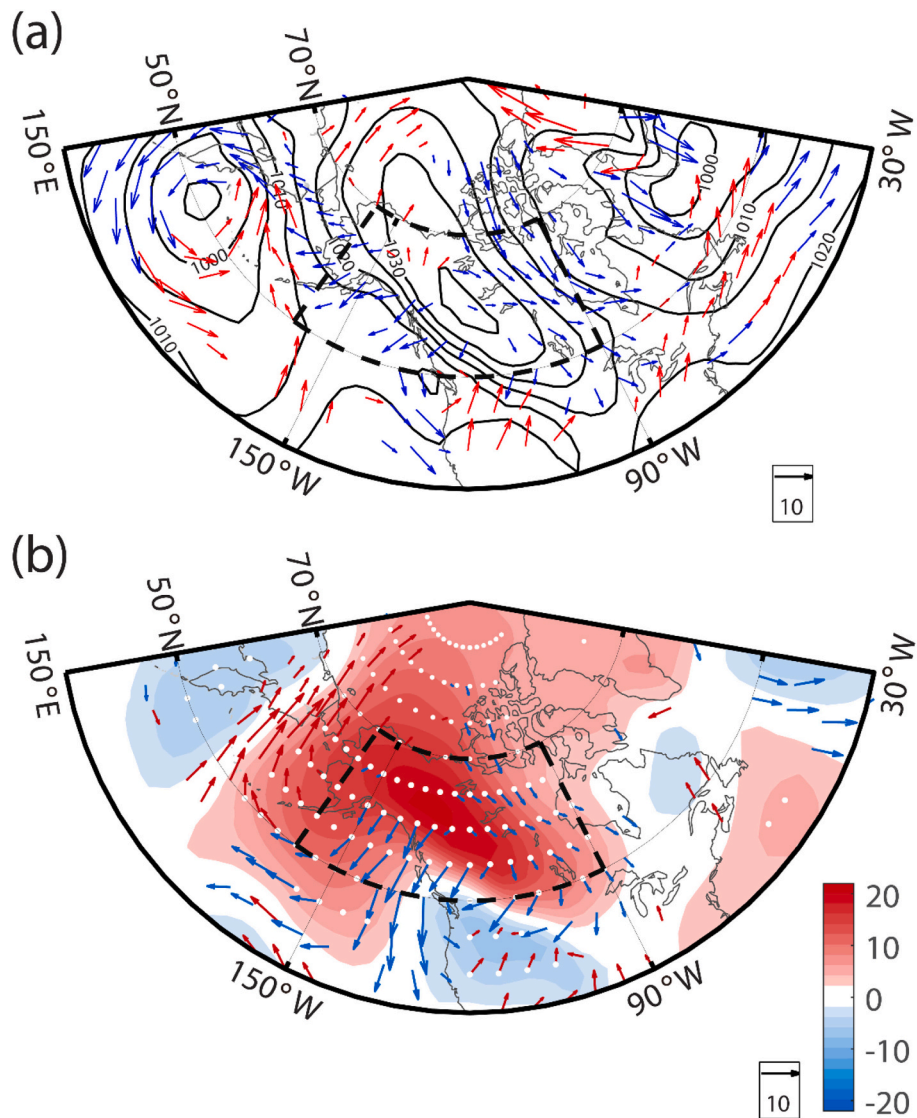
Fig. 5. Composite (a) SLP (contour, 5hPa interval) and winds (vector, in m/s) at 10m, and (b) SLP anomalies (shading, in hPa) and wind anomalies (vector, in m/s) at 10m on the day with the maximum coverage of each event. White dots in (b) indicate the areas exceeding 95% confidence level for SLP anomalies. All the plotted vectors indicate either zonal or meridional component exceeding 95% confidence level of student's *t*-test. The black dashed lines outline the NWNA region.
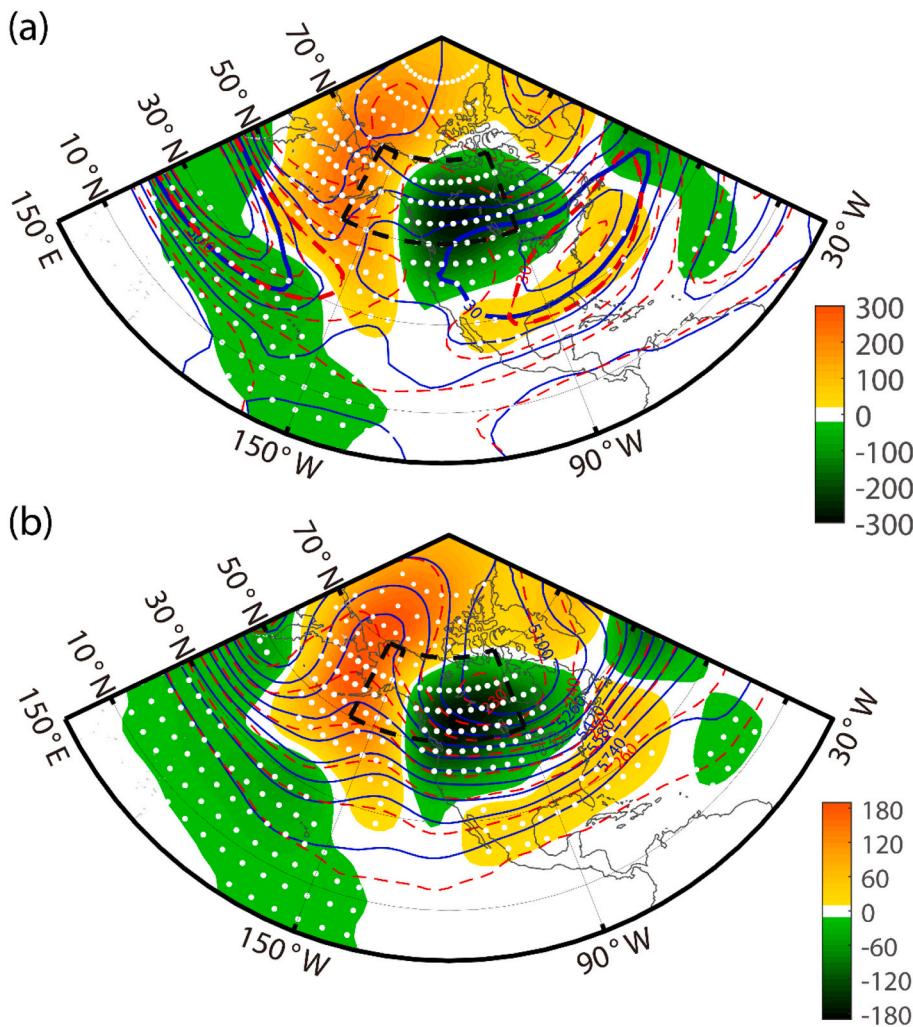
Fig. 6. Composite (a) geopotential height anomalies (shading, in gpm), zonal winds (blue contour, 8m/s interval), and corresponding daily climatological zonal winds (red contour, 8m/s interval) at 300hPa and (b) geopotential height anomalies (shading, in gpm), total height (blue contour, 80gpm interval), and total temperature (red contour, 5°C interval) at 500hPa on the day with the maximum coverage of each event. White dots indicate the areas exceeding 95% confidence level for height anomalies. The black dashed lines outline the NWNA region. In (a), contours of 30m/s are highlighted to indicate the jet stream.

Table 2

Composite values of synchronous daily circulation/teleconnection index for the wintertime cold events in the NWNA. Note that the symbol "*" and "**" denote the index value exceeding 90% and 95% confidence level of student's *t*-test, respectively.

Teleconnection			Circulation		
PNA	AO	NAO	Arctic cell	Polar cell	Ferrel cell
-0.46**	-0.90**	0.03	0.76	4.5*	-2.5

on this issue. To explore whether the early SIC condition during September and October has a delayed influence (Francis et al., 2009; Jaiser et al., 2012) as a precursor for the wintertime cold events over NWNA, we plot the composite SIC anomalies in Arctic region averaged over the two months (Fig. 11a). Results show a dipole pattern with positive anomalies in East Siberian Sea, Chukchi Sea, and Beaufort Sea and negative anomalies in Barents Sea and Kara Sea. However, this distribution is not statistically significant (Fig. 11a), indicating a non-robust relationship between cold extremes in NWNA and SIC in Arctic region. We conduct similar calculations for the snow cover during October and November (Fig. 11b). Again, no significant linkage is detected between the snow cover in NA continent and wintertime cold extremes in NWNA. We did not investigate the effect of Eurasian snow cover on NWNA cold extremes (Cohen and Jones, 2011). Besides, there are no significant synchronal anomalies of Arctic SIC and snow cover in NA continent associated with the cold extremes (not shown).

6. Summary and discussion

In this paper, we have analyzed the cold extremes located in NWNA (50–70°N, 90–160°W), which not only is a crucial genesis location for Arctic air mass and its associated anticyclone but also has great implication for the weather prediction in eastern NA. Based on our comprehensive criteria in terms of intensity, coverage, and duration, we totally select 23 cold events from 1981 to 2018. The strongest event occurred in 1990 from 27 January to 17 February, lasting for 22 days with the maximum area-mean intensity at around -19°C. Specifically, we calculate the interannual variation of integrated intensity of cold events in NWNA and highlight a significant weakening trend.

From surface up to 850hPa, the Beaufort anticyclone stretches southward and merges with the continental anticyclone over NA. This intensified and meridional-elongated anticyclone drives strong northerlies and cold advections over the NWNA region. As previous studies did not focus on the upper troposphere, we specially notice a robust mid-latitude wave train including a strong low anomaly over NWNA and an anomalous high ridge over northeast Pacific extending into the Arctic region at 300hPa. Note that the relationship between the planetary waves and cold outbreaks is complex and location dependent (Screen and Simmonds, 2013, 2014). The above low anomaly extends from lower troposphere to stratosphere, which exactly centers at around 250–300hPa. The deep cold anomaly under the low-pressure system is prominent at surface corresponding to the cold extremes in NWNA. Moreover, the jet stream becomes stronger due to stronger temperature and height gradients and moves northwestwards because of the
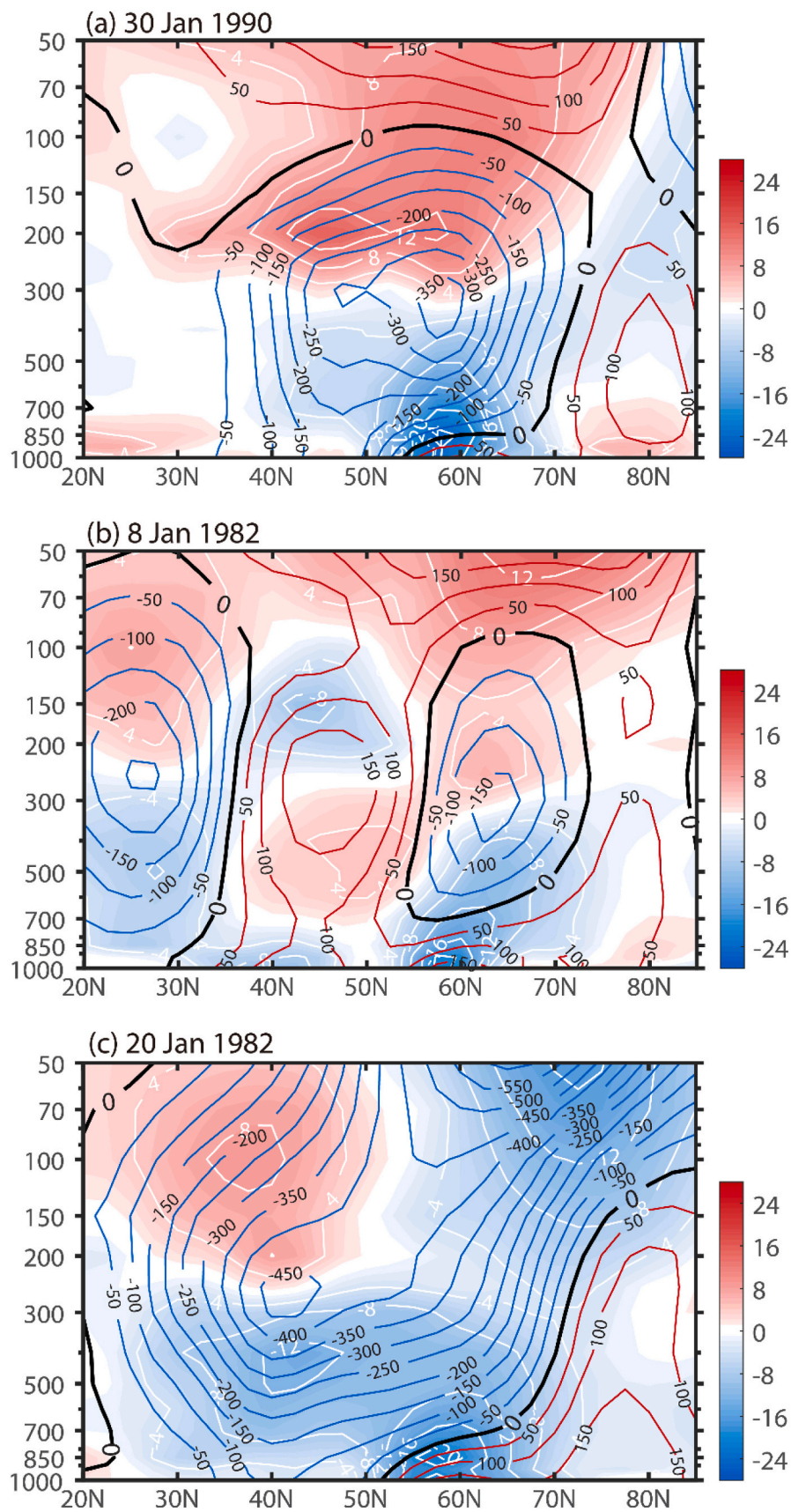
Fig. 7. The cross section of geopotential height (blue and red contour, 50gpm interval) and temperature anomalies (shading with white contour, 4°C interval) along 120°W on the day with the maximum coverage of the top three strongest cold events.
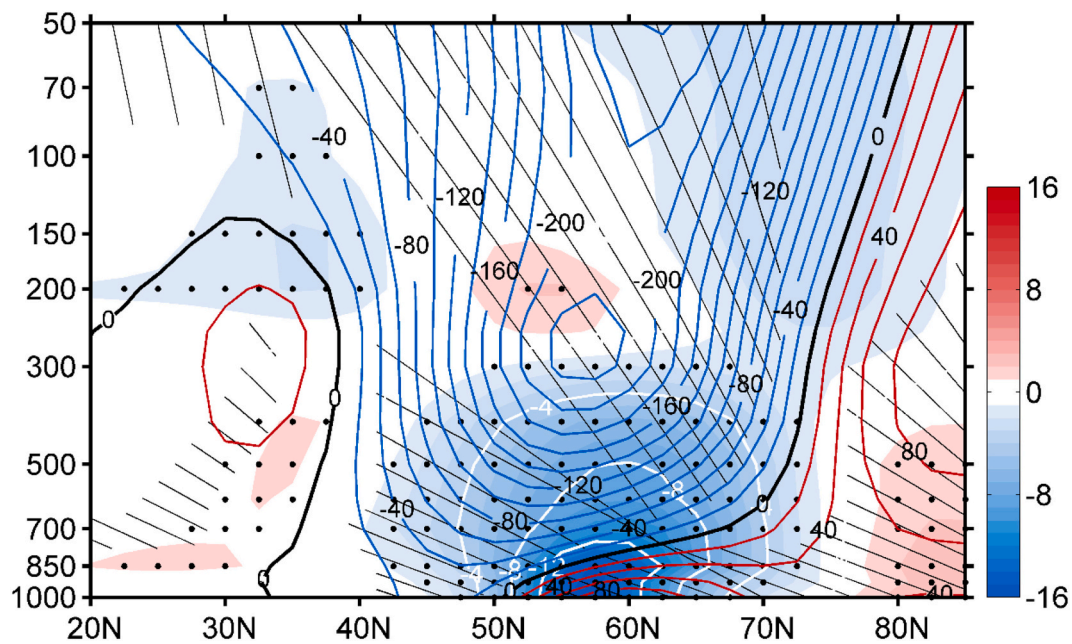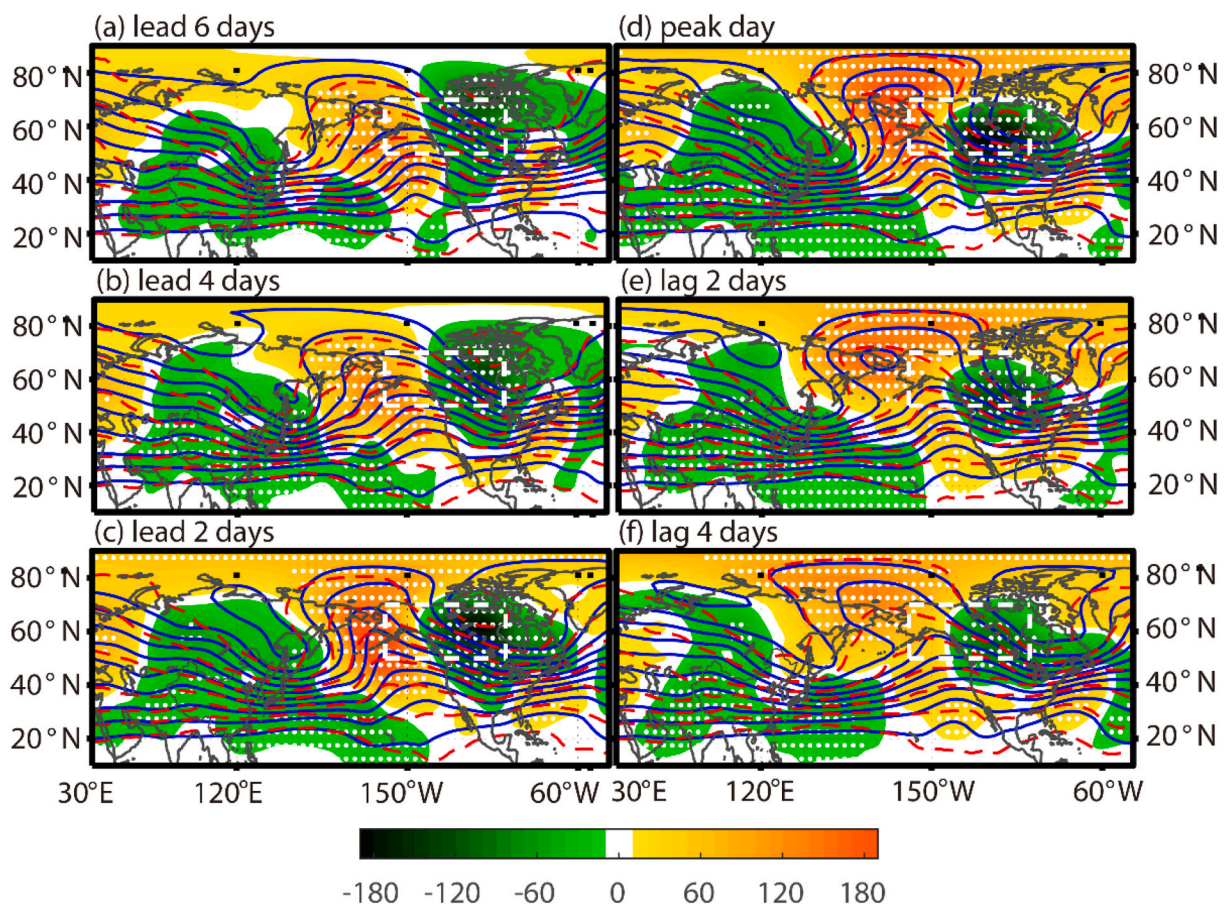
Fig. 8. The composite cross section of geopotential height (blue and red contour, 20gpm interval) and temperature anomalies (shading with white contour, 4°C interval) along 120°W averaged over the lifetime of all events. Black slashes for height anomalies and dots for temperature anomalies indicate the areas exceeding 95% confidence level.

Fig. 9. Composite evolution of geopotential height anomalies (shading, in gpm), total height (blue contour, 80gpm interval), and total temperature (red contour, 5°C interval) at 500hPa from leading (a) 6, (b) 4, (c) 2, (d) 0 to lagging (e) 2, (f) 4 days relative to the peak day. White dots indicate the areas exceeding 95% confidence level for height anomalies. The white dashed lines outline the NWNA region.
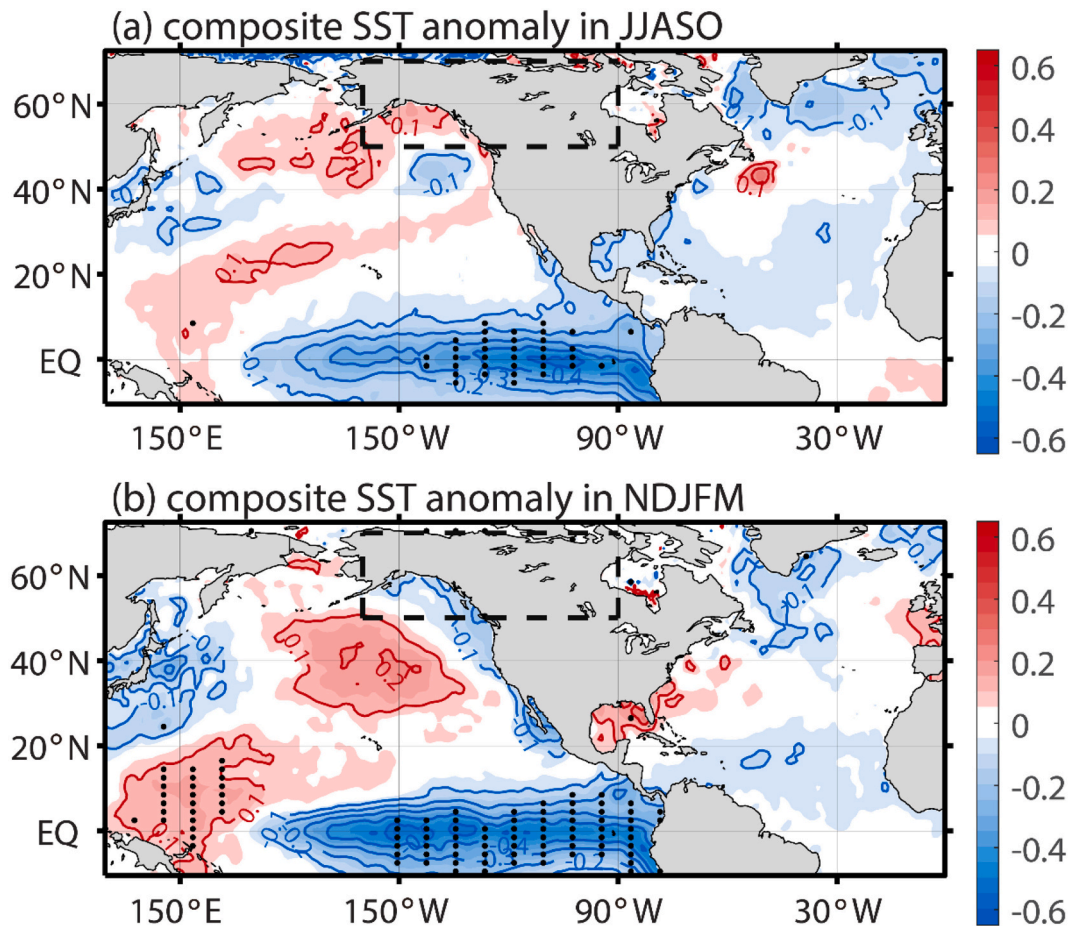
Fig. 10. Composite SST anomalies (shading with contour, in °C) averaged over (a) June-July-August-September-October (JJASO; the summer and autumn before the cold extremes) and (b) November-December-January-February-March (NDJFM; the winter of the cold extremes). Black dots indicate the areas exceeding 95% confidence level. The black dashed lines outline the NWNA region.

northwestward movement of the Alaska ridge. At 500hPa, the enhanced blocking high extends into the central Arctic region, driving strong cold advection into NWNA. Moreover, there is a significant PNA-like teleconnection originating from tropical Pacific and propagating towards Aleutian Islands, NWNA, and southern NA. The general opposite height anomalies in polar and mid-latitude regions indicate a negative phase of AO. The potential connection between the cold extremes in NWNA and meridional cells is also investigated. Results show a significantly reinforced zonally-averaged Polar cell, which is not the case for the sectorial-averaged Polar cell.

Results suggest that the La Niña-like SST anomalies may serve as a precursor and favorable background for the cold extremes in NWNA. The La Niña-like SST anomalies can trigger a PNA-like wave train including a negative height anomaly center located above the NWNA, which is linked with the negative temperature anomalies extending downward to the surface. The optimal juxtaposition of local and remote factors operating on multiple timescales is required to generate a cold

extreme (e.g., Dole et al., 2014). However, the SIC anomalies in Arctic region and the snow cover in NA continent during early months reveal no significant linkage with the wintertime cold extremes in NWNA.

In recent studies, radiation and moisture are found to be pivotal during the lifetime of cold extremes in NWNA (e.g., Turner et al., 2013; Cassano et al., 2016) and other regions in NH (Lee et al., 2017; Luo et al., 2017). We should further examine their roles as well as the changes of large-scale meteorological patterns in past and future cold extremes.

Declaration of Competing Interest

The authors declare that they have no known competing financial interests or personal relationships that could have appeared to influence the work reported in this paper.

(a) composite sea ice concentration anomaly in Sep-Oct
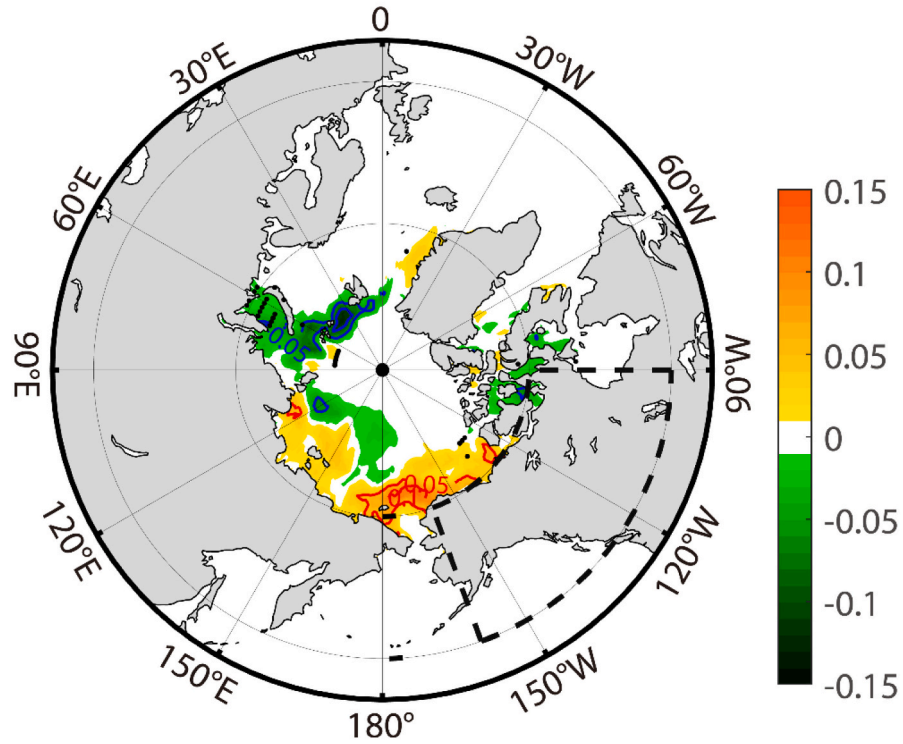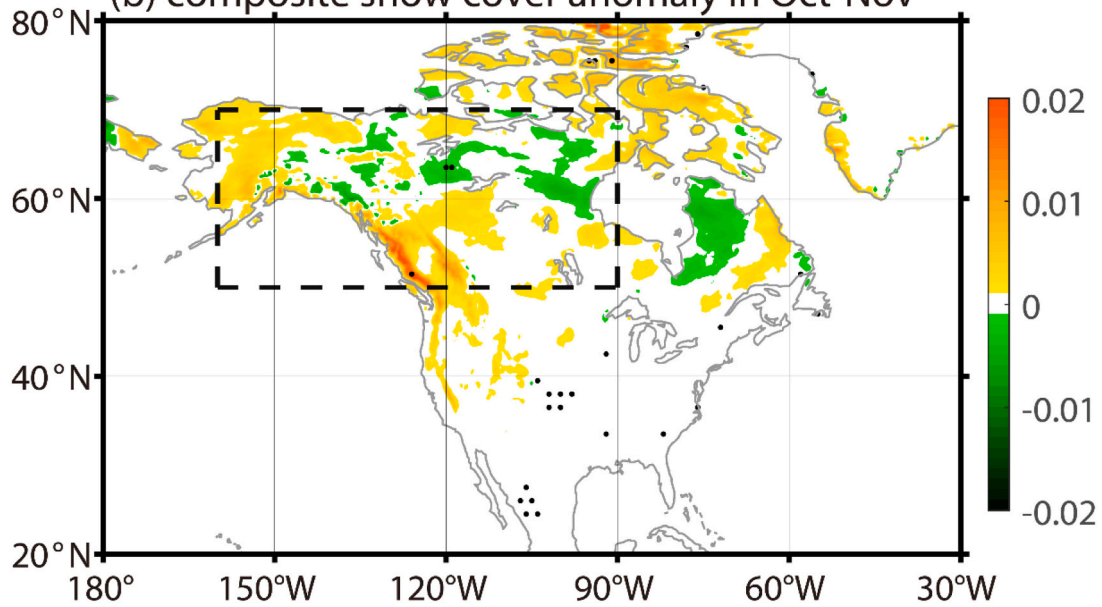
(b) composite snow cover anomaly in Oct-Nov

Fig. 11. Same as Figure 10a, but for (a) SIC anomalies during September-October and (b) snow cover anomalies (unit: meter) in October-November.

Acknowledgments

References

Barnston, A.G., Livezey, R.E., 1987. Classification, seasonality and persistence of low-frequency atmospheric circulation patterns. Mon. Weather Rev. 115, 1083–1126.

Blackport, R., Screen, J.A., van der Wiel, K., Bintanja, R., 2019. Minimal influence of reduced Arctic sea ice on coincident cold winters in mid-latitudes. Nat. Clim. Chang. 9, 697–704.

Cassano, E.N., Cassano, J.J., Nolan, M., 2011. Synoptic weather pattern controls on temperature in Alaska. J. Geophys. Res. Atmos. 116, D11108.

Cassano, J.J., Cassano, E.N., Seefeldt, M.W., Gutowski Jr., W.J., Glisan, J.M., 2016. Synoptic conditions during wintertime temperature extremes in Alaska. J. Geophys. Res. Atmos. 121, 3241–3262.

Castruccio, F.S., Ruprich-Robert, Y., Yeager, S.G., Danabasoglu, G., Msadek, R., Delworth, T.L., 2019. Modulation of Arctic sea ice loss by atmospheric teleconnections from Atlantic multidecadal variability. J. Clim. 32, 1419–1441.

Cattiaux, J., Vautard, R., Cassou, C., Yiou, P., Masson-Delmotte, V., Codron, F., 2010. Winter 2010 in Europe: A cold extreme in a warming climate. Geophys. Res. Lett. 37, L20704.

Chen, W.Y., van den Dool, H., 2003. Sensitivity of teleconnection patterns to the sign of their primary action center. Mon. Weather Rev. 131, 2885–2899.

Cohen, J., Jones, J., 2011. A new index for more accurate winter predictions. Geophys. Res. Lett. 38, L21701.

Cohen, J., Barlow, M., Kushner, P., Saito, K., 2007. Stratosphere–troposphere coupling and links with Eurasian land-surface variability. J. Clim. 20, 5335–5343.

Cohen, J., Jones, J., Furtado, J.C., Tziperman, E., 2013. Warm Arctic, cold continents: A common pattern related to Arctic sea ice melt, snow advance, and extreme winter weather. Oceanography 26, 150–160.

Cohen, J., Screen, J.A., Furtado, J.C., Barlow, M., Whittleston, D., Coumou, D., Francis, J., Dethloff, K., Entekhabi, D., Overland, J., Jones, J., 2014. Recent Arctic amplification and extreme mid-latitude weather. Nat. Geosci. 7, 627–637.

Coumou, D., Rahmstorf, S., 2012. A decade of weather extremes. Nat. Clim. Chang. 2, 491–496.

Derome, J., Brunet, G., Plante, A., Gagnon, N., Boer, G.J., Zwiers, F.W., Lambert, S.J., Sheng, J., Ritchie, H., 2001. Seasonal predictions based on two dynamical models. Atmos.-Ocean 39, 485–501.

Dole, R., Hoerling, M., Kumar, A., Eischeid, J., Perlwitz, J., Quan, X.W., Kiladis, G., Webb, R., Murray, D., Chen, M., Wolter, K., 2014. The making of an extreme event: Putting the pieces together. Bull. Am. Meteorol. Soc. 95, 427–440.

Emanuel, K., 2008. Back to Norway: An essay. In: Synoptic—Dynamic Meteorology and Weather Analysis and Forecasting, Meteor. Monogr. 55. American Meteorological Society, Boston, MA, pp. 87–96.

Francis, J.A., Vavrus, S.J., 2012. Evidence linking Arctic amplification to extreme weather in mid-latitudes. Geophys. Res. Lett. 39, L06801.

Francis, J.A., Chan, W., Leathers, D.J., Miller, J.R., Veron, D.E., 2009. Winter Northern Hemisphere weather patterns remember summer Arctic sea-ice extent. Geophys. Res. Lett. 36, L07505.

Gao, Y., Leung, L.R., Lu, J., Masato, G., 2015. Persistent cold air outbreaks over North America in a warming climate. Environ. Res. Lett. 10, 044001.

Gerber, F., Sedláček, J., Knutti, R., 2014. Influence of the western North Atlantic and the Barents Sea on European winter climate. Geophys. Res. Lett. 41, 561–567.

Gleason, K.L., Lawrimore, J.H., Levinson, D.H., Karl, T.R., Karoly, D.J., 2008. A revised US climate extremes index. J. Clim. 21, 2124–2137.

Grotjahn, R., Black, R., Leung, R., Wehner, M.F., Barlow, M., Bosilovich, M., Gershunov, A., Gutowski, W.J., Gyakum, J.R., Katz, R.W., Lee, Y.Y., 2016. North American extreme temperature events and related large scale meteorological patterns: A review of statistical methods, dynamics, modeling, and trends. Clim. Dyn. 46, 1151–1184.

Guirguis, K., Gershunov, A., Schwartz, R., Bennett, S., 2011. Recent warm and cold daily winter temperature extremes in the Northern Hemisphere. Geophys. Res. Lett. 38, L17701.

Hersbach, H., Bell, B., Berrisford, P., et al., 2020. The ERA5 global reanalysis. Q. J. R. Meteorol. Soc. 146, 1999–2049.

Honda, M., Inoue, J., Yamane, S., 2009. Influence of low Arctic sea-ice minima on anomalously cold Eurasian winters. Geophys. Res. Lett. 36, L08707.

Horton, D.E., Johnson, N.C., Singh, D., Swain, D.L., Rajaratnam, B., Diffenbaugh, N.S., 2015. Contribution of changes in atmospheric circulation patterns to extreme temperature trends. Nature 522, 465–469.

Hu, Y., Fu, Q., 2007. Observed poleward expansion of the Hadley circulation since 1979. Atmos. Chem. Phys. 7, 5229–5236.

Hurrell, J.W., 1995. Decadal trends in the North Atlantic Oscillation: Regional temperatures and precipitation. Science 269, 676–679.

Itoh, H., 2008. Reconsideration of the true versus apparent Arctic Oscillation. J. Clim. 21, 2047–2062.

Jaiser, R., Dethloff, K., Handorf, D., Rinke, A., Cohen, J., 2012. Impact of sea ice cover changes on the Northern Hemisphere atmospheric winter circulation. Tellus A 64, 11595.

Jones, P.D., Moberg, A., 2003. Hemispheric and large-scale surface air temperature variations: An extensive revision and an update to 2001. J. Clim. 16, 206–223.

Kanamitsu, M., Ebisuzaki, W., Woollen, J., Yang, S.K., Hnilo, J.J., Fiorino, M., Potter, G. L., 2002. NCEP–DOE AMIP-II Reanalysis (R-2). Bull. Am. Meteorol. Soc. 83, 1631–1644.

Kodra, E., Steinhaeuser, K., Ganguly, A.R., 2011. Persisting cold extremes under 21st-century warming scenarios. Geophys. Res. Lett. 38, L08705.

Kug, J.S., Jeong, J.H., Jang, Y.S., Kim, B.M., Folland, C.K., Min, S.K., Son, S.W., 2015. Two distinct influences of Arctic warming on cold winters over North America and East Asia. Nat. Geosci. 8, 759–762.

Kumar, A., Perlwitz, J., Eischeid, J., Quan, X., Xu, T., Zhang, T., Hoerling, M., Jha, B., Wang, W., 2010. Contribution of sea ice loss to Arctic amplification. Geophys. Res. Lett. 37, L21701.

Lee, S., Gong, T., Feldstein, S.B., Screen, J., Simmonds, I., 2017. Revisiting the cause of the 1989–2009 Arctic surface warming using the surface energy budget: Downward infrared radiation dominates the surface fluxes. Geophys. Res. Lett. 44, 10654–10661.

Li, C., Stevens, B., Marotzke, J., 2015. Eurasian winter cooling in the warming hiatus of 1998–2012. Geophys. Res. Lett. 42, 8131–8139.

Li, M., Luo, D., Simmonds, I., Dai, A., Zhong, L., Yao, Y., 2020. Anchoring of atmospheric teleconnection patterns by Arctic sea ice loss and its link to winter cold anomalies in East Asia. Int. J. Climatol. In press.

Lin, H., Brunet, G., 2009. The influence of the Madden–Julian oscillation on Canadian wintertime surface air temperature. Mon. Weather Rev. 137, 2250–2262.

Lindzen, R.S., Hou, A.V., 1988. Hadley circulations for zonally averaged heating centered off the equator. J. Atmos. Sci. 45, 2416–2427.

Liu, J., Curry, J.A., Wang, H., Song, M., Horton, R.M., 2012. Impact of declining Arctic sea ice on winter snowfall. Proc. Nat. Acad. Sci. 109, 4074–4079.

Luo, B., Luo, D., Wu, L., Zhong, L., Simmonds, I., 2017. Atmospheric circulation patterns which promote winter Arctic sea ice decline. Environ. Res. Lett. 12, 054017.

Luo, D., Chen, X., Dai, A., Simmonds, I., 2018. Changes in atmospheric blocking circulations linked with winter Arctic warming: A new perspective. J. Clim. 31, 7661–7678.

Luo, D., Chen, X., Overland, J., Simmonds, I., Wu, Y., Zhang, P., 2019. Weakened potential vorticity barrier linked to recent winter arctic sea ice loss and midlatitude cold extremes. J. Clim. 32, 4235–4261.

Luo, B., Luo, D., Dai, A., Simmonds, I., Wu, L., 2020. Combined influences on North American winter air temperature variability from North Pacific blocking and the North Atlantic Oscillation: Subseasonal and interannual time scales. J. Clim. 33, 7101–7123.

Mitas, C.M., Clement, A., 2005. Has the Hadley cell been strengthening in recent decades? Geophys. Res. Lett. 32, L03809.

Mo, K.C., 2010. Interdecadal modulation of the impact of ENSO on precipitation and temperature over the United States. J. Clim. 23, 3639–3656.

Mori, M., Watanabe, M., Shiogama, H., Inoue, J., Kimoto, M., 2014. Robust Arctic sea-ice influence on the frequent Eurasian cold winters in past decades. Nat. Geosci. 7, 869–873.

van Oldenborgh, G.J., Mitchell-Larson, E., Vecchi, G.A., de Vries, H., Vautard, R., Otto, F., 2019. Cold waves are getting milder in the northern midlatitudes. Environ. Res. Lett. 14, 114004.

Overland, J.E., Wood, K.R., Wang, M., 2011. Warm Arctic-cold continents: Climate impacts of the newly open Arctic Sea. Polar Res. 30, 15787.

Papineau, J.M., 2001. Wintertime temperature anomalies in Alaska correlated with ENSO and PDO. Int. J. Climatol. 21, 1577–1592.

Peings, Y., Brun, E., Mauvais, V., Douville, H., 2013. How stationary is the relationship between Siberian snow and Arctic Oscillation over the 20th century? Geophys. Res. Lett. 40, 183–188.

Perlwitz, J., Hoerling, M., Dole, R., 2015. Arctic tropospheric warming: Causes and linkages to lower latitudes. J. Clim. 28, 2154–2167.

Peterson, T.C., et al., 2013. Monitoring and understanding changes in heat waves, cold waves, floods, and droughts in the United States: State of knowledge. Bull. Am. Meteorol. Soc. 94, 821–834.

Portis, D.H., Cellitti, M.P., Chapman, W.L., Walsh, J.E., 2006. Low-frequency variability and evolution of North American cold air outbreaks. Mon. Weather Rev. 134, 579–597.

Qian, W., Wu, K., Chen, D., 2015a. The Arctic and Polar cells act on the Arctic sea ice variation. Tellus A 67, 27692.

Qian, W., Chen, Y., Jiang, M., Hu, Q., 2015b. An anomaly-based method for identifying signals of spring and autumn low-temperature events in the Yangtze River valley. China. J. Appl. Meteorol. Climatol. 54, 1216–1233.

Qian, W., Wu, K., Leung, J.C.H., 2016. Three-dimensional structure and long-term trend of heat wave events in western Eurasia revealed with an anomaly-based approach. Int. J. Climatol. 36, 4315–4326.

Qian, W., Wu, K., Leung, J.C.H., 2017. Climatic anomalous patterns associated with the Arctic and Polar cell strength variations. Clim. Dyn. 48, 169–189.

Rayner, N.A., Parker, D.E., Horton, E.B., Folland, C.K., Alexander, L.V., Rowell, D.P., Kent, E.C., Kaplan, A., 2003. Global analyses of sea surface temperature, sea ice, and night marine air temperature since the late nineteenth century. J. Geophys. Res. Atmos. 108, 4407.

Ropelewski, C.F., Halpert, M.S., 1986. North American precipitation and temperature patterns associated with the El Niño/Southern Oscillation (ENSO). Mon. Weather Rev. 114, 2352–2362.

Screen, J.A., Simmonds, I., 2013. Caution needed when linking weather extremes to amplified planetary waves. Proc. Nat. Acad. Sci. 110, E2327.

Screen, J.A., Simmonds, I., 2014. Amplified mid-latitude planetary waves favour particular regional weather extremes. Nat. Clim. Chang. 4, 704–709.

Screen, J.A., Deser, C., Sun, L., 2015. Reduced risk of North American cold extremes due to continued Arctic sea ice loss. Bull. Am. Meteorol. Soc. 96, 1489–1503.

Serreze, M.C., Francis, J.A., 2006. The Arctic amplification debate. Climatic Chang. 76, 241–264.

Shi, J., Qian, W., 2016. Connection between anomalous zonal activities of the South Asian High and Eurasian summer climate anomalies. J. Clim. 29, 8249–8267.

Sillmann, J., Croci-Maspoli, M., Kallache, M., Katz, R.W., 2011. Extreme cold winter temperatures in Europe under the influence of North Atlantic atmospheric blocking. J. Clim. 24, 5899–5913.

Smith, E.T., Sheridan, S.C., 2018. The characteristics of extreme cold events and cold air outbreaks in the eastern United States. Int. J. Climatol. 38, e807–e820.

Smith, E.T., Sheridan, S.C., 2020. Where do Cold Air Outbreaks occur and how have they changed over time? Geophys. Res. Lett. 47 e2020GL086983.

Stroeve, J.C., Kattsov, V., Barrett, A., Serreze, M., Pavlova, T., Holland, M., Meier, W.N., 2012. Trends in Arctic sea ice extent from CMIP5, CMIP3 and observations. Geophys. Res. Lett. 39, L16502.

Sun, L., Perlwitz, J., Hoerling, M., 2016. What caused the recent "Warm Arctic, Cold Continents" trend pattern in winter temperatures? Geophys. Res. Lett. 43, 5345–5352.

Thompson, D.W., Wallace, J.M., 2001. Regional climate impacts of the Northern Hemisphere annular mode. Science 293, 85–89.

Titchner, H.A., Rayner, N.A., 2014. The Met Office Hadley Centre sea ice and sea surface temperature data set, version 2: 1 Sea ice concentrations. J. Geophys. Res. Atmos. 119, 2864–2889.

Turner, J.K., Gyakum, J.R., 2011. The development of Arctic air masses in Northwest Canada and their behavior in a warming climate. J. Clim. 24, 4618–4633.

Turner, J.K., Gyakum, J., Milrad, S.M., 2013. A thermodynamic analysis of an intense North American arctic air mass. Mon. Weather Rev. 141, 166–181.

Urrego-Blanco, J.R., Hunke, E.C., Urban, N., 2019. Emergent relationships among sea ice, longwave radiation, and the Beaufort High circulation exposed through parameter uncertainty analysis. J. Geophys. Res. Oceans 124, 9572–9589.

Vavrus, S., 2007. The role of terrestrial snow cover in the climate system. Clim. Dyn. 29, 73–88.

Vavrus, S., Walsh, J.E., Chapman, W.L., Portis, D., 2006. The behavior of extreme cold air outbreaks under greenhouse warming. Int. J. Climatol. 26, 1133–1147.

Wallace, J.M., 2000. North Atlantic oscillation/annular mode: Two paradigms—one phenomenon. Q. J. Roy. Meteor. Soc. 126, 791–805.

Walsh, J.E., Phillips, A.S., Portis, D.H., Chapman, W.L., 2001. Extreme cold outbreaks in the United States and Europe, 1948–99. J. Clim. 14, 2642–2658.

Wang, C., Liu, H., Lee, S.K., 2010. The record-breaking cold temperatures during the winter of 2009/2010 in the Northern Hemisphere. Atmos. Sci. Lett. 11, 161–168.

Westby, R.M., Lee, Y.Y., Black, R.X., 2013. Anomalous temperature regimes during the cool season: Long-term trends, low-frequency mode modulation, and representation in CMIP5 simulations. J. Clim. 26, 9061–9076.

Wheeler, D.D., Harvey, V.L., Atkinson, D.E., Collins, R.L., Mills, M.J., 2011. A climatology of cold air outbreaks over North America: WACCM and ERA-40 comparison and analysis. J. Geophys. Res. Atmos. 116, D12107.

Wu, Q., Zhang, J., Zhang, X., Tao, W., 2014. Interannual variability and long-term changes of atmospheric circulation over the Chukchi and Beaufort seas. J. Clim. 27, 4871–4889.

Yao, Y., Luo, D., Dai, A., Simmonds, I., 2017. Increased quasi-stationarity and persistence of winter Ural blocking and Eurasian extreme cold events in response to Arctic warming Part I: Insights from observational analyses. J. Clim. 30, 3549–3568.

Yu, J.Y., Zou, Y., Kim, S.T., Lee, T., 2012. The changing impact of El Niño on US winter temperatures. Geophys. Res. Lett. 39, L15702.

Zhang, M., Perrie, W., Long, Z., 2019. Decadal variations in the winter Beaufort High and the stratospheric polar vortex. Geophys. Res. Lett. 46, 4933–4941.

Zishka, K.M., Smith, P.J., 1980. The climatology of cyclones and anticyclones over North America and surrounding ocean environs for January and July, 1950–77. Mon. Weather Rev. 108, 387–401.